Pramana – J. Phys. (2022) 96:81
https://doi.org/10.1007/s12043-022-02326-x

Pressure- and temperature-dependent EIT studies in a parabolic quantum dot coupled with excitonic effects in a static magnetic field

MONICA GAMBHIR[1],*, VARSHA[2,3] and VINOD PRASAD[1]

[1]Department of Physics, Swami Shraddhanand College, University of Delhi, Delhi 110 036, India
[2]Department of Physics and Astrophysics, University of Delhi, Delhi 110 007, India
[3]Department of Physics, Kalindi College, University of Delhi, Delhi 110 008, India
*Corresponding author. E-mail: monicagambhir@ss.du.ac.in

MS received 14 August 2021; revised 27 November 2021; accepted 11 December 2021

Abstract. The present paper analyses the electromagnetically-induced transparency (EIT) in a three-level ladder-type system in an excitonic three-dimensional quantum dot (QD) with a parabolic potential in the presence of a static magnetic field, a resonant probe field and a coupler field. Eigenvalues, wave functions, dipole matrix elements and selection rules of the quantum system are calculated analytically within the effective mass approximation by solving the corresponding Schrödinger equation and taking into consideration both the confinement and Coulomb potentials of the electron–hole pair. To illustrate the interaction with the optical fields, the analytical expressions for the complex electric susceptibility, absorption, dispersion, group index (GI) and the combined effects of external factors such as magnetic field, hydrostatic pressure, temperature and dimensions of the QD are examined.

Keywords. Quantum dot; exciton; magnetic field; non-linear effects; electromagnetically-induced transparency; susceptibility; absorption; dispersion; group index.

PACS Nos 42.55.-f; 78.66.-w; 73.21.-La

1. Introduction

Electronic and optical studies in semiconductor heterostructures have gathered considerable attention due to versatile device applications. Various studies have been carried out on III–V semiconductor heterostructures, particularly, GaAs/$Ga_{1-x}Al_xAs$ semiconductor systems. The strong interaction of these heterostructure systems with light induces novel optical phenomena that are important to comprehend the conceptual physics underlying non-linear optics in these structures. The presence of manifold transition pathways, inhomogeneous broadening, enhanced nonlinear optical properties, design flexibility, ease of synthesis, etc. motivate researchers to study interesting phenomena including non-linear optical properties [1,2], Rashba spin–orbit coupling [3], STIRAP [4], terahertz signal detection [5], Kerr nonlinearity [6], etc. in various semiconductor systems. Electromagnetically-induced transparency (EIT) is one of those phenomena where, using quantum interference effects, an ultranarrow transparency window (TW) opens up to a probe field beam in the presence of a strong coupling laser. The study of EIT allows for many new applications, including quantum information processing [7], efficient non-linear mixing [8], nanosensor [9,10], refractive index sensor [11], slow-light device [12] and optical switch [13] to name a few. The process of EIT was first found theoretically and was then established experimentally by Imamoğlu *et al* [14,15] in atomic systems. Thereafter, both theoretical and experimental researchers have written various research papers based on the study of EIT in semiconductor quantum nanostructures. Phillips and Wang [16] reported experimental studies of EIT arising from exciton spin coherence in the transient optical response of GaAs quantum wells. Gumber *et al* studied EIT in the two-dimensional quantum ring and its application in enhancing the output of the sum-frequency generation process [18]. Niculescu discussed the effect of the electric field process of EIT in a quantum disk under highly intense laser radiation [19]. Bejan has discussed the effect of electric and magnetic fields on the occurrence of EIT in a double quantum dot (QD) system [20,21]. Very recently, Sahebi *et al* investigated EIT in a four-level C-model of GaAs cylindrical QD with parabolic potential [17].

Published online: 11 April 2022

Among the aforementioned optical phenomena, those related to exciton are onerous to treat theoretically due to the inadequacy of analytical expressions for the wave functions corresponding to the bound states of electron–hole pairs. Excitons in quantum nanostructures have the advantage of having discrete energy levels with the benefits of large electric dipole moments and high nonlinear optical coefficients. Electric dipole transitions between excitonic states are in the THz range. Hence, excitonic structures reveal a strong response to applied external fields. Based on these properties, various studies on excitonic quantum nanostructures that emphasise the interaction of excitons with high-intensity THz laser fields have been submitted [5,22–24]. In the present paper, EIT is investigated in an excitonic three-dimensional QD with a parabolic potential in the presence of an external static magnetic field, wherein a coupling laser resonantly couples a low-lying excitonic ground level, to one or higher levels, thereby inducing EIT for a probe beam that measures absorption between two electric dipole forbidden energy levels. This transparency is a consequence of the destructive interference between the two excitation routes. While destructive interference decreases the linear susceptibility, the non-linear susceptibility experiences constructive interference in the spectral region of induced transparency of the medium and hence is associated with steep dispersion. Excitonic systems have Coulomb-bound states that can be greatly altered by applied external fields, hydrostatic pressure, temperature, etc. The hydrostatic pressure amends the band-gap structure and energy shift occurs without amending the structure of quantum nanostructure and the non-linear optical response can be greatly enhanced by changing external pressure and temperature. The hydrostatic pressure variations of the physical properties are beneficial for exploring the new phenomena and have been considered both experimentally and theoretically [25–29]. In addition to the impact of hydrostatic pressure and temperature on the process of EIT induced in our QD system, we have also studied the impact of strong confinement and weak confinement of exciton in QD. Altogether, we have presented a wide, broad and systematic overview of EIT in our excitonic system. The method of EIT examined in this paper can be used for realising various optoelectronic devices such as all-optical switches, photovoltaic cells, light-emitting diodes and modulators for the wavelength ranges consistent with the excitonic transitions in QD.

The structure of the research paper is as follows: Section 2 briefly presents the model of QD and the theory of EIT. We have calculated the expressions of Hamiltonian, the appropriate wave functions, energy levels, dipole matrix elements and selection rules for the allowed transitions. The process of EIT is explained and analytical expressions for susceptibility and group index (GI) are obtained using the time evolution density matrix equation. Variation of effective masses, band gap and EIT with external factors, specifically pressure and temperature are also presented. In §3 the procured results for variation in external factors and field, size of QD and study of EIT with and without Coulomb interaction and discussion of these results are reported. Finally, §4 gives the main conclusion of our research paper.

2. Model and theory

2.1 *Exciton in a quantum dot*

An exciton is a bound state of an electron and a hole with more closely matched effective masses, bound to each other by the electrostatic Coulomb force of attraction. Inside a QD, an exciton is formed when a material absorbs a photon having energy more than its band gap. This excites an electron from the valence band into the conduction band. This formation is analogous to the hydrogen atom with discrete energy states. The transition energies in the excitonic QD systems are close to the meV range. Accordingly, they can be controlled by the external fields that stimulate transitions in this range. We study an exciton confined in a three-dimensional $GaAs/Al_xGa_{1-x}$ QD with a parabolic confinement potential. In the presence of a transverse magnetic field, the Hamiltonian, employing the effective mass approximation can be expressed as

$$H = \frac{1}{2m_e^*}\left(\vec{p}_e + \frac{e\vec{A}_e}{c}\right)^2 + \frac{1}{2}m_e^*\omega_e^2 r_e^2 + \frac{1}{2m_h^*}\left(\vec{p}_h - \frac{e\vec{A}_h}{c}\right)^2 + \frac{1}{2}m_h^*\omega_h^2 r_h^2 - \frac{e^2}{\varepsilon_r\,|\vec{r}_e - \vec{r}_h|}. \quad (1)$$

Here, e is the free electron charge, c is the speed of light in free space and $m^*_{e(h)}$ is the effective mass of the electron (hole), ω_e and ω_h are, respectively, the confinement frequencies of the electron and the hole and ε_r is the dielectric constant of the medium. Both $m^*_{e(h)}$ and ε_r are dependent on pressure and temperature variations. The positions of electron and hole are described by vectors $\vec{r}_e$ and $\vec{r}_h$. The eigenvalues and wave functions of the whole Hamiltonian are calculated using the method of numerical diagonalisation of Hamiltonian explained in detail in our recent research paper [30]. Here we give a brief overview of the computation of energy eigenvalues, selection rules for allowed transitions between

any two excitonic states and the corresponding non-zero dipole matrix elements.

The total Hamiltonian can be separated into relative coordinate $\vec{r}$ and the centre-of-mass coordinate (c.m.) $\vec{R}$, defined by

$$\vec{R} = (m_e^*\vec{r}_e + m_h^*\vec{r}_h)/M.$$

We define

$$M = m_e^*M + m_h^*M \text{ and } \mu = \frac{m_e^*m_h^*}{M}$$

as the total and reduced mass, respectively. With the symmetric gauge for the magnetic field, $\vec{A}_e = -\vec{A}_h = \vec{A} = \frac{1}{2}(\vec{B} \times \vec{r})$ the total Hamiltonian becomes

$$\begin{aligned} H = &\frac{P^2}{2M} + \frac{p^2}{2\mu} + \frac{e^2A^2}{2\mu c^2} \\ &+\frac{e}{c}\left(\frac{\vec{P}}{M} - \frac{1}{2}\left(\frac{1}{m_h^*} - \frac{1}{m_e^*}\right)\vec{p}\right)\cdot\vec{A} \\ &+\frac{e}{c}\vec{A}\cdot\left(\frac{\vec{P}}{M} - \frac{1}{2}\left(\frac{1}{m_h^*} - \frac{1}{m_e^*}\right)\vec{p}\right) \\ &+\frac{1}{2}m_e^*\omega_e^2r_e^2 + \frac{1}{2}m_h^*\omega_h^2r_h^2 - \frac{e^2}{\varepsilon_r\vec{r}}, \end{aligned} \tag{2}$$

where

$$\omega_r^2 = \frac{m_h^{*2}}{M^3}\left(m_h^*\omega_e^2 + m_e^*\omega_h^2\right),$$
$$\omega_R^2 = \frac{M}{m_e^{*2}}\left(m_h^*\omega_h^2 + m_e^*\omega_e^2\right).$$

Decomposing the full Hamiltonian and using the atomic units everywhere ($\hbar = e = m_e = \frac{1}{4\pi\varepsilon_0} = 1$) as

$$H = H_{\text{cm}} + H_{\text{rel}} + H_{\aleph} + H_C, \tag{3}$$

where

$$H_{\text{cm}} = \frac{m_e^*}{M}H_R^0.$$

Here

$$\begin{aligned} H_R^0 &= \frac{P^2}{2m_e^*} + \frac{m_e^*}{2}\omega_R^2R^2 \\ H_{\text{rel}} &= \frac{p^2}{2\mu} + \frac{e^2A^2}{2\mu c^2} + \frac{e}{2}\left(\frac{1}{m_e^*} - \frac{1}{m_h^*}\right)(\vec{p}\cdot\vec{A} + \vec{A}\cdot\vec{p}) \\ &\quad + \frac{Mm_e^*}{2m_h^*}\omega_r^2r^2 - \frac{e^2}{\varepsilon_r r} \\ H_{\aleph} &= \frac{m_e^*m_h^*}{M}\left(\omega_e^2 - \omega_h^2\right)\vec{R}\cdot\vec{r} + \frac{2e}{M}\vec{P}\cdot\vec{A}. \end{aligned}$$

H_{cm}, H_{rel}, $H_{\aleph}$ and H_C denote the c.m., relative and cross term of the Hamiltonian, respectively. $H_{\aleph}$ is the cross term Hamiltonian consisting of both c.m. and relative coordinates and H_C is the electrostatic-interaction term between the electron and the hole. Using spherical polar coordinates (r, θ, ϕ) in the symmetric gauge, wherein $A_r = A_\theta = 0$ and

$$A_\phi = \frac{Br\sin\theta}{2}$$

H_{rel} can be simplified to

$$\begin{aligned} H_{\text{rel}} = \frac{M}{m_h^*}\Bigg[&\frac{-1}{2m_e^*}\left\{\frac{1}{r^2}\frac{\partial}{\partial r}\left(r^2\frac{\partial}{\partial r}\right)\right. \\ &\left.-\frac{L^2}{r^2} + i\left(\frac{m_h^* - m_e^*}{M}\right)\omega_b\frac{\partial}{\partial\phi}\right\} \\ &+\frac{r^2}{2m_e^*}\left(\frac{\omega_b^2}{4} + m_e^{*2}\omega_r^2\right) \\ &-\frac{\omega_b^2r^2}{8m_e^*}\cos^2\theta - \frac{m_h^*}{M}\frac{1}{\varepsilon_r r}\Bigg], \end{aligned} \tag{4}$$

where $\omega_b = eB$. H_{rel} can be further fragmented as

$$H_{\text{rel}} = \frac{M}{m_e^*m_h^*}H_r^0 + H_r^I + H_C$$

and

$$H_{\text{rel}}^I = -\frac{M}{8m_e^*m_h^*}\omega_b^2r^2\cos^2\theta,\ H_C = -\frac{1}{\varepsilon_r r}$$

and H_r^0 contains all the terms independent of B. The full Hamiltonian can be resolved into two parts: unperturbed Hamiltonian,

$$H_0 = \frac{m_e^*}{M}H_R^0 + \frac{M}{m_e^*m_h^*}H_r^0$$

and perturbed Hamiltonian

$$H_I = H_r^I + H_{\aleph} + H_C.$$

The eigenvalues and wave functions of the whole Hamiltonian are calculated using the method of numerical diagonalisation of the Hamiltonian. The following expressions for the eigenvalue and eigenfunction for the unperturbed relative Hamiltonian H_r^o are obtained:

$$E_{nlm}^0 = \left(2n + l + \frac{3}{2}\right)\Omega_r + \frac{m\omega_b}{2}\left(\frac{m_h^* - m_e^*}{M}\right) \tag{5}$$

$$\begin{aligned} \psi_{nlm}(\rho, \theta, \phi) = &C_{nl}\rho^{-1/4}W_M^r\left(\nu, l', \rho\right) \\ &\times Y_{lm}(\theta, \phi) \end{aligned} \tag{6}$$

where

$$C_{nl} = \sqrt{\frac{2\Omega_r^{3/2}\left(n + l + \frac{1}{2}\right)!}{n!\left(l + \frac{1}{2}\right)!^2}},$$

$$\Omega_r^2 = \frac{\omega_b^2}{4} + m_e^{*2}\omega_r^2$$

and

$$\nu = \frac{2E_{nlm}^0}{4\Omega_r} - \frac{m\omega_b}{4\Omega_r}\left(\frac{m_h^* - m_e^*}{M}\right)$$

and eigenvalues and eigenfunctions for the unperturbed c.m. Hamiltonian H_R^0 are obtained as

$$E_{NLM}^0 = \left(2N + L + \frac{3}{2}\right)\frac{\Omega_R}{m_e^*} \tag{7}$$

$$\mathrm{X}_{NLM}(P,\ \Theta,\ \Phi) = C_{NL}P^{-1/4}W_M^R\left(\Upsilon, L',\ P\right) \times Y_{L,M}(\Theta,\ \Phi), \tag{8}$$

where

$$L' = \frac{1}{4}(1 + 2L), \quad \Omega_R = Mm_e^*\omega_R$$

and

$$\Upsilon = \frac{E_{NLM}^0}{2\Omega_R}$$

so that the unperturbed energies are

$$E^0 = E_{nlm}^0 + E_{NLM}^0 \tag{9}$$

with unperturbed wave function given by the product of c.m. and relative wave function

$$\Psi_{\mathcal{NLM}n\ell m} = X_{NLM}(P, \Theta, \Phi)\,\psi_{nlm}(\rho, \theta, \phi). \tag{10}$$

$\Psi_{\mathcal{NLM}n\ell m}$ acts as a basis wave function to find the total wave functions for the whole system.

The interaction of excitonic QD system with a linearly polarised periodic electromagnetic radiation (angular frequency ω and direction of polarisation z) is of the form

$$\vec{E}(t) = 2\vec{E}_0\cos(\omega t) = \vec{E}_0(\mathrm{e}^{i\omega t} + \mathrm{e}^{-i\omega t}).$$

The electric dipole transition matrix element between any two states i and f is obtained by solving the matrix element

$$M_{fi} = \langle i \mid -\vec{\mu}\cdot\vec{E} \mid f\rangle = \langle nlm \mid E_0 er\cos\theta \mid n'l'm'\rangle = \langle er\rangle E_0 \int \mathrm{d}(\cos\theta)\mathrm{d}\phi Y_{l,m}^* C_{1,0} Y_{l',m'} \tag{11}$$

$C_{p,q}$ are reduced spherical harmonics given by

$$C_{p,q} = \sqrt{\frac{4\pi}{2p+1}}Y_{p,q}.$$

Integrals involving the reduced spherical harmonics are related to the Wigner 3-j symbols related to Clebsch–Gordan coefficients. The integral in eq. (11) can be solved to obtain

$$M_{fi} = e\int r^2\mathrm{d}r\xi_{nl}(r)\,r\xi_{n'l'}(r')\sqrt{(2l+1)(2l'+1)} \times \begin{pmatrix} l & 1 & l' \\ 0 & 0 & 0 \end{pmatrix}\begin{pmatrix} l & 1 & l' \\ -m & 0 & m' \end{pmatrix}. \tag{12}$$

Only those transitions are dipole allowed for which electric dipole moment and hence values of Wigner 3-j symbols are non-zero. Based on this analysis, we find the following selection rules for allowed optical transitions: $l + l' + 1 =$ even and $m = m$.

Various theoretical studies of excitons confined in spherical QDs with parabolic potentials have been reported. The key aspect of these researches is that the same confinement frequency of the parabolic potential for both the electron and the hole is chosen by the authors. However, the dimension of QD depends on both the carriers confined in regions of space with unlike radii. In this context, we describe the dimension of QD using the length scale $L{=}\sqrt{L_eL_h}$ where

$$L_{e(h)}{=}\sqrt{\frac{\hbar}{\mu\omega_{e(h)}}}.$$

To determine the type of confinement of the exciton, we can compare it with the exciton Bohr radius

$$a_B^*{=}\frac{\varepsilon_r\hbar^2}{\mu e^2}.$$

If the Coulomb term related to the relative coordinates is very small and can be neglected, i.e., $L{\leq}a_B^*$, we get the strong confinement limit (SCL). In this limit, Coulomb term is dealt with as a perturbation and electrons and holes show uncorrelated behaviour. If the Coulomb interaction leads the state of the exciton, we get the weak confinement limit (WCL), $L{\geq}a_B^*$, i.e., the QD radius is greater than the Bohr radius of both electron and hole. This situation corresponds to large-sized QDs.

2.2 *EIT formalism*

Let us consider the internal dynamics of the system to be described by a three-level ladder-type or cascade configuration provided by the exciton levels in the introduced QD system: the ground state $|g\rangle$ and the excited states $|e_1\rangle$ and $|e_2\rangle$. The system is assumed to be initially in the ground state. The transitions between three levels are initiated by two laser beams, the probe laser field ω_p and the coupling laser field ω_c as illustrated in figure 1.

The probe beam measures the absorption spectra for the transition between the ground state $|g\rangle$ and the excited state $|e_1\rangle$ and the applied strong coupler beam couples the energy states $|e_1\rangle$ and $|e_2\rangle$. In this scheme, the transition between the states $|g\rangle$ and the excited

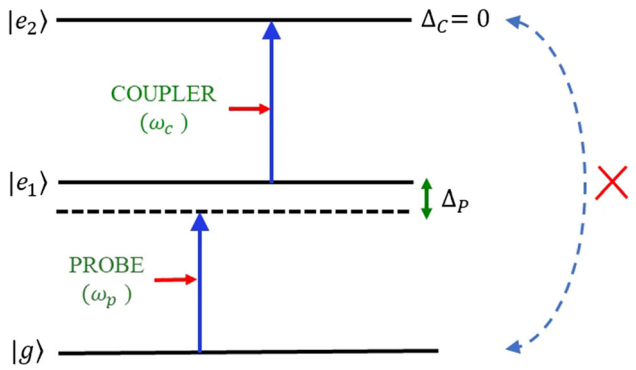

Figure 1. Three-level ladder scheme for realising EIT in excitonic QD system.

states $|e_2\rangle$ is forbidden by the dipole interaction of the electric field and transitions between $|g\rangle \rightarrow |e_1\rangle$ and $|e_1\rangle \rightarrow |e_2\rangle$ are dipole allowed. In EIT, generally, when an electromagnetic field of frequency equal to $\omega_{g,e1}$ is applied, excitons in the ground state $|g\rangle$ can absorb energy and transit to the state $|e_1\rangle$. But, when a coupling electromagnetic field resonant with the $|e_1\rangle \rightarrow |e_2\rangle$ transition is also applied, there are two transition pathways by which an exciton can get from the ground state to the excited state: the transition can be either in the same way as earlier, or along $|g\rangle \rightarrow |e_1\rangle \rightarrow |e_2\rangle$. These two allowed transition routes can destructively interfere, and under a suitable environment, this results in zero probe absorption at resonance. This interference effect, making an opaque medium transparent, is the core of EIT. Mathematically, the whole process in the excitonic ladder system can be understood by the general results obtained as follows:

The net applied electric field is the superposition of the probe and the coupler beams:

$$\vec{E}(t) = \vec{E}_p(t)\cos\omega_p(t) + \vec{E}_c(t)\cos\omega_c(t).$$

$$\Omega_p = \frac{E_p\left|\mu_{g,e1}\right|}{\hbar}$$

and

$$\Omega_c = \frac{E_c\left|\mu_{e1,e2}\right|}{\hbar}$$

are the rf Rabi frequencies for the probe and the coupling fields, respectively. If $\hbar\omega_{ij}$ is the energy difference between the levels i and j then $\Delta_p = \omega_p - \omega_{g,e1}$ and $\Delta_c = \omega_c - \omega_{e1,e2}$ are the respective detuning between the field and the corresponding transition. Here, $\hbar\omega_{ij}$ is the energy difference between the levels i and j. Assuming that wavelengths of the probe and the coupler beams are considerably longer than the effective dimensions of QD, the electric dipole approximation is invoked and electric fields are assumed to be independent of the coordinate term.

To describe the interaction with the optical fields and a model three-level system, we solve the equation of motion for the density matrix for the stationary QD system. The time evolution of the populations of the states is governed by the Liouville equation

$$\frac{\partial\rho}{\partial t} = \frac{1}{i\hbar}\langle n\,|\,[H_0 + H_I, \rho]\,|\,m\rangle - \frac{1}{2}\{\Gamma, \rho\}, \tag{13}$$

where Γ is the relaxation matrix defined for any state as $\Gamma = \gamma_m\,|m\rangle\,\langle m|$. γ's can be related to the rate at which the different elements of the density matrix ρ thermalise. Total Hamiltonian of the QD system is given by

$$H = H_0 + H_I(t), \tag{14}$$

where H_0 represents the unperturbed Hamiltonian and $H_I = \vec{\mu}\cdot\vec{E}(t)$ describes the interaction between the system and the probe-coupler beams. Here, $\mu_{nm} = \langle n\,|\,\vec{\mu}\,|\,m\rangle\cdot\hat{\varepsilon_i}$ where $|m\rangle$ is an eigenket of H_0 and $\hat{\varepsilon_i}$ is a unit vector along the direction of the electromagnetic field propagation. For a spherically symmetric system, $\mu_{gg} = \mu_{e1,e1} = \mu_{e2,e2} = 0$. We have also assumed that the transition between the states $|g\rangle$ and the excited states $|e_2\rangle$ is forbidden by dipole interaction of the electric field, i.e. $\mu_{g,e_2} = 0$.

Using the dipole and rotating wave approximations, the evolution of this system in a steady state can be described by the density matrix formalism [31,32]

$$\rho_{e1,g} = -\frac{i[\Omega_p\left(\rho_{g,g} - \rho_{e1,e1}\right) - \Omega_c^*\rho_{e2,g}]}{2\left(\gamma_{e1,g} - i\Delta_p\right)} \tag{15}$$

$$\rho_{e2,e1} = -\frac{i[\Omega_c\left(\rho_{e2,e2} - \rho_{e1,e1}\right) + \Omega_p^*\rho_{e2,g}]}{2\left(\gamma_{e2,e1} - i\Delta_c\right)} \tag{16}$$

$$\rho_{e2,g} = -\frac{i[\Omega_p\rho_{e2,e1} - \Omega_c\rho_{e1,g}]}{2[\gamma_{e2,g} - i\left(\Delta_p + \Delta_c\right)]} \tag{17}$$

$$\rho_{e1,e1} = \frac{i}{2\Gamma_{e1}}(\Omega_p^*\rho_{e1,g} - \Omega_p\rho_{g,e1}) \tag{18}$$

and

$$\rho_{e2,e2} = \frac{i}{2\Gamma_{e2}}\left(\Omega_c^*\rho_{e2,e1} - \Omega_c\rho_{e1,e2}\right). \tag{19}$$

With the strong coupler beam, Gea-Banacloche *et al* [33] showed that only $\rho_{e1,g}$ will contribute to the dispersion and absorption of the medium. This is experimentally achievable by exposing the system to the coupler laser for some time before the probe laser is switched on, the dispersion and the absorption are calculated by solving in an adiabatic regime. The expression so obtained is

$$\rho_{e1,g} = \frac{i\Omega_p}{2\left(i\Delta_p - \gamma_{e1,g}\right) + \frac{|\Omega_c|^2}{2i(\Delta_p+\Delta_c)-\text{cc}}} \tag{20}$$

and this is related to the complex susceptibility $\chi(\omega_p) = \chi_1 + i\chi_2$ as

$$\chi = -\frac{2\sigma\mu_{e1,g}^2\rho_{e1,g}}{\varepsilon_0\hbar\Omega_p}. \tag{21}$$

Here, σ is the density of excitons. With simpler algebra, the final expression for the real and imaginary parts of χ is obtained as follows:

$$\chi_1 = \frac{\sigma\mu_{e1,g}^2}{\varepsilon_0\hbar} \times \left(\frac{-\Delta_p + \frac{G}{\gamma_{e2,g}}}{\left(-\Delta_p + \frac{G}{\gamma_{e2,g}}\right)^2 + \left(\gamma_{e1,g} + \frac{G}{(\Delta_p - \Delta_c)}\right)^2} \right), \tag{22}$$

$$\chi_2 = \frac{\sigma\mu_{e1,g}^2}{\varepsilon_0\hbar} \times \left(\frac{\gamma_{e1,g} + \frac{G}{\Delta_p - \Delta_c}}{\left(-\Delta_p + \frac{G}{\gamma_{e2,g}}\right)^2 + \left(\gamma_{e1,g} + \frac{G}{(\Delta_p - \Delta_c)}\right)^2} \right), \tag{23}$$

where

$$G = \frac{|\Omega_c|^2 \gamma_{e2,g} (\Delta_p - \Delta_c)}{4[(\Delta_p - \Delta_c)^2 + \gamma_{e2,g}^2]}.$$

The real and imaginary parts of $\chi(\omega_p)$ describe absorption coefficient (AC), $\alpha(\omega_p)$, and the refractive index (RI) or (dispersion), $n_r(\omega_p)$, from the relations

$$\alpha(\omega_p) = \frac{\omega_p}{c}\chi_2(\omega_p) \tag{24}$$

$$n_r(\omega_p) = 1 + \frac{1}{2}\chi_1(\omega_p). \tag{25}$$

When the frequency of a particular transition is consistent with the frequency of incident radiation, a resonance phenomenon happens. Light propagation is then supplemented by strong absorption and dispersion. Harris and Hau [34] observed that sizeable dispersion of refractive index in the EIT window can be used to lessen the group velocity of light pulses up to $10-10^2$ m/s [35]. When a light pulse enters a dispersive linear medium, the light pulse propagates at the group velocity

$$v_g = \frac{c}{n_g},$$

where

$$v_g = \frac{c}{1 + n_r(\omega_p) + \omega_p \frac{\partial}{\partial\omega_p} n_r(\omega_p)} \tag{26}$$

and n_g is the group refractive index given by

$$n_g = 1 + \frac{\chi_1}{2} + \frac{\omega_p}{2}\frac{\partial\chi_1}{\partial\omega_p}. \tag{27}$$

It can be observed that v_g depends on χ_1 and its derivatives. When χ_1 is zero, and the dispersion is very steep and positive, the group velocity is significantly reduced, i.e., subluminal ($v_g < c$) which is slow light for $n_g > 1$. However, when the dispersion is anomalous, i.e., superluminal, $|n_g| < 1$. The negative slope of dispersion corresponds to superluminal light propagation, while the positive slope shows subluminal light propagation [36]. Consequently, the group velocity of a pulse passing through a medium can even be faster than the velocity of light in vacuum, c, without challenging the causality principle.

2.3 *The effects of hydrostatic pressure and temperature*

The hydrostatic pressure alters the band structure of the heterostructure and leads to changes in the properties of the elementary excitations of the heterostructure systems. The application of hydrostatic pressure and temperature modifies the effective mass, dielectric constant, band gap and hence, size of QD. The explicit expressions for these quantities as a function of the hydrostatic pressure and temperature [37,38] can be written as

$$\frac{m_e^*(P,T)}{m_e} = \left[1 + E_P^\Gamma \left\{ 2E_g^\Gamma(P,T)^{-1} + \left(E_g^\Gamma(P,T) + \Delta_0\right)^{-1} \right\}\right], \tag{28}$$

where $m_e^*(P,T)$ is the pressure- and temperature-dependent free-electron mass, E_P^Γ is the energy related to momentum-matrix element, $\Delta_0 = 0.341$ eV is the spin–orbit splitting. $E_g^\Gamma(P,T)$ is the pressure- and temperature-dependent energy gap for GaAs at the Γ-point in units of eV given by

$$E_g^\Gamma(P,T) = E_g^\Gamma(0,T) + \alpha P + \beta P^2, \tag{29}$$

where

$$\alpha = 1.26 \times 10^{-2}\,\text{eV kbar}^{-1},$$
$$\beta = 3.77 \times 10^{-5}\,\text{eV kbar}^{-2},$$
$$E_g^\Gamma(0,T) = 1.519 - \frac{5.405 \times 10^{-4} T^2}{T + 204}\text{eV}.$$

The effective mass of $Al_xGa_{1-x}As$ is: $m_b^*(P,T) = m_d^*(P,T) + 0.083x$. Here, x denotes the aluminium

content. The hydrostatic pressure- and temperature-dependent valence band effective mass is given by

$$\frac{m_h^*(P,T)}{m_h} = \left(0.09 - 0.20 \times 10^{-3} P - 3.55 \times 10^{-5} T\right). \quad (30)$$

The pressure- and temperature-dependent static dielectric constant of GaAs is written as

$$\varepsilon(P,T) = \begin{cases} 12.74 \exp\left(-1.73 \times 10^{-3} P\right) \exp\left[9.4 \times 10^{-5} (T - 75.6)\right] \text{ for } T < 200\,\text{K} \\ 13.18 \exp\left(-1.73 \times 10^{-3} P\right) \exp\left[20.4 \times 10^{-5} (T - 300)\right] \text{ for } T > 200\,\text{K} \end{cases} \quad (31)$$

In the next section, we present and discuss our results obtained for the phenomena of EIT with variation in external magnetic field, pressure, temperature and dimensions of QD.

3. Numerical results and discussion

In the following, we shall discuss the effects of confinement, external magnetic field, hydrostatic pressure and temperature on EIT and GI of an exciton confined in a typical three-dimensional spherical GaAs/$Al_xGa_{1-x}As$ QD with a parabolic confinement potential exposed to probe-coupler beams. For numerical calculations, we utilised the following material parameters: effective mass of the electron (e) and heavy hole (hh) at zero pressure and temperature are, respectively, $m_e^* = 0.067m_0$ and $m_{hh}^* = 0.377m_0$ (m_0 is the free electron mass), $\sigma = 1 \times 10^{20}\,\text{m}^{-3}$, $\gamma_{e2,g} = (0.01\,\text{ps})^{-1}$, $\varepsilon_0 = 8.85 \times 10^{-12}\,\text{Fm}^{-1}$. For all the calculations $\omega_e = 2\omega_h$, $\gamma_{e1,g} = 10^{-4}\gamma_{e2,g}$ and the size of QD is approx. 10 nm, unless otherwise stated. To examine the EIT effect, we focus on the real and imaginary parts of susceptibility, χ_1 and χ_2, respectively. The real and imaginary parts of susceptibilities are proportional to dispersion and absorption, respectively, as can be calculated using eqs (22) and (23). The levels considered to study the process of EIT are $|320300\rangle$, $|320310\rangle$ and $|320320\rangle$. The transition between the levels $|320300\rangle$ corresponding to the ground state $|g\rangle$ and $|320320\rangle$ corresponding to the excited state $|e_2\rangle$ are forbidden based on the selection rules. Hence, the electric dipole matrix element $\mu_{g,e_2} = 0$ for transitions between the states with the same parity. In the beginning, it is important to note that the energy level separations $\Delta_{e1,g}$ and the squared dipole matrix elements $\mu_{e1,g}^2$ are the primary parameters that affect the position and crest values of susceptibility curves, respectively.

In figure 2, we illustrate the effects of rabi frequency on χ_1 and χ_2. As can be observed, χ_2 and hence absorption is maximum when the coupler laser field is turned off ($\Omega_c = 0$) and only the probe field is applied.

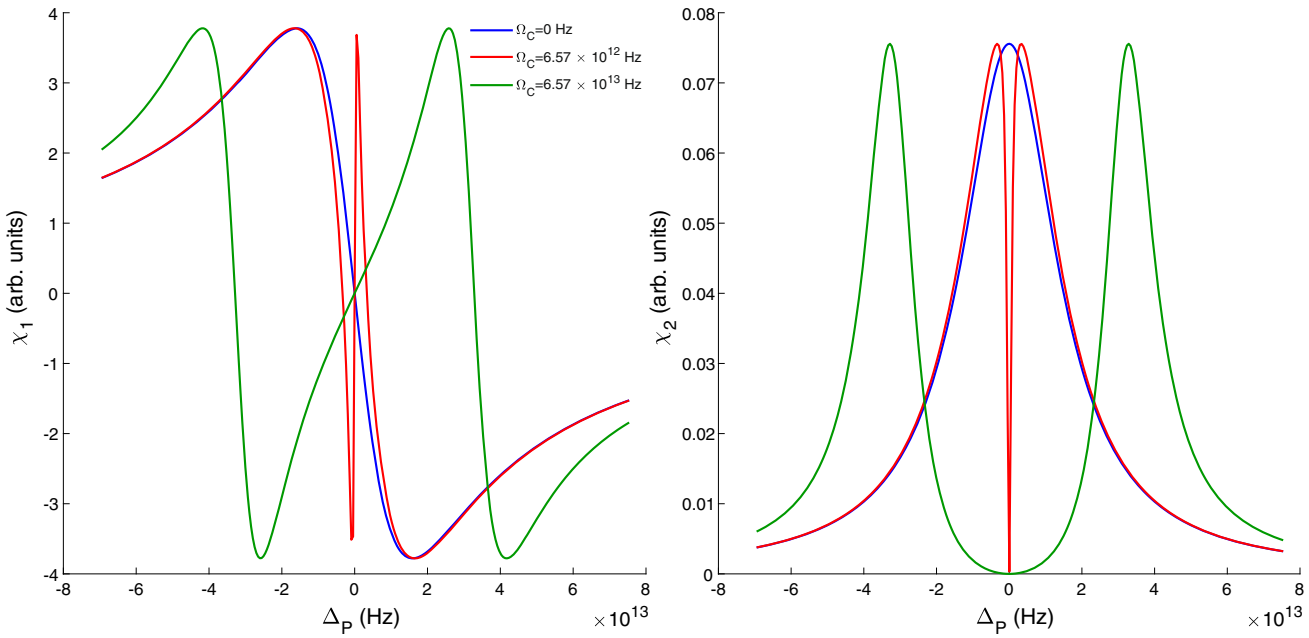

Figure 2. Variation of χ_1 and χ_2 with detuning of the probe field for different rabi frequencies Ω_C.

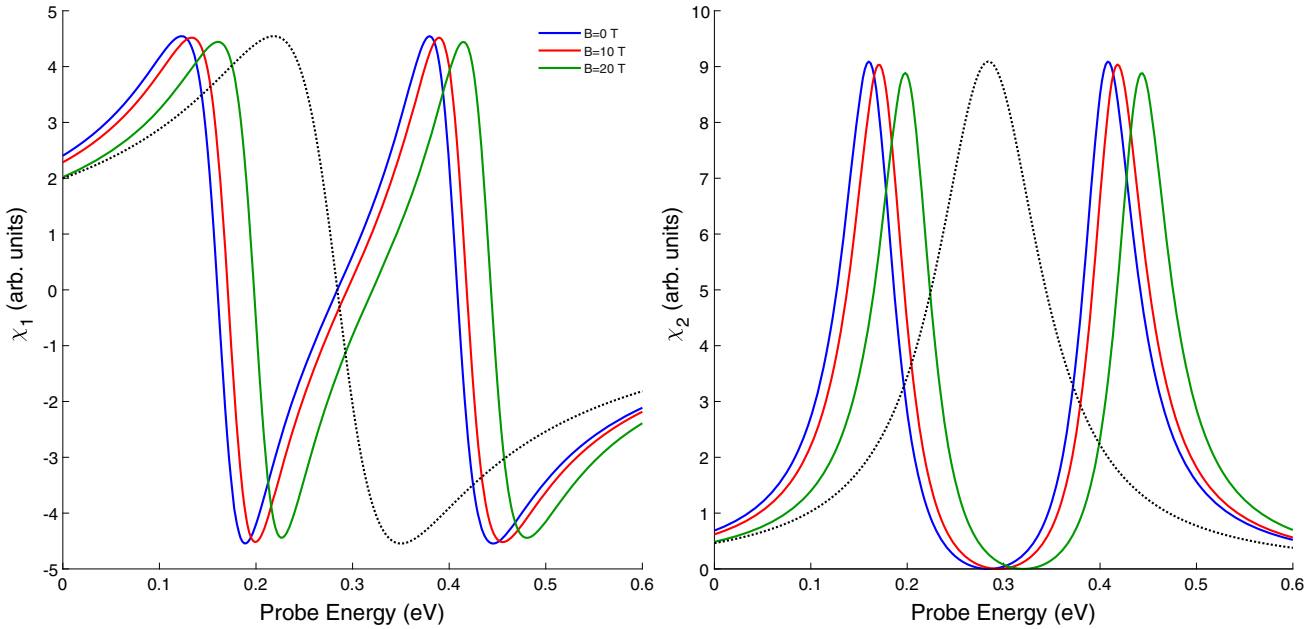

Figure 3. Variation of χ_1 and χ_2 with the energy of the probe field for different magnetic field strengths.

Further, the real and imaginary parts of the susceptibility are given by

$$\chi_1 = \frac{\sigma \mu_{e1,g}^2}{\varepsilon_0 \hbar} \left(\frac{-\Delta_p}{-\Delta_p^2 + \gamma_{e1,g}^2} \right)$$

$$\chi_2 = \frac{\sigma \mu_{e1,g}^2}{\varepsilon_0 \hbar} \left(\frac{\gamma_{e1,g}}{-\Delta_p{}^2 + \gamma_{e1,g}^2} \right).$$

χ_2 has a Lorentzian shape with a maximum value when the probe field is in resonance with energy levels so that $\Delta_p = 0$. At this point, χ_2 attains zero value. As the coupler field is ignited with detuning $\Delta_c = 0$ (to ensure the greatest absorption), a transparency interface gets opened up in the opaque quantum system, the absorption depicts a doublet and resembles an Autler Townes doublet centred on $\Delta_p = 0$. It is observed that χ_1 and χ_2 become zero at specific probe frequencies which means that the absorption is zero and the refractive index closely equals unity. However, the restricted transparency resonance is supplemented by a very abrupt variation of the refractive index with the frequency of the probe field. Hence, the medium changes to a transparent medium for the coupler light. The population of the atoms gets confined in the lowest state, making it a dark state preserving the other two states virtually unoccupied.

The influence of magnetic field, B, on the absorption and dispersion profiles of the quantum system is shown in figure 3, keeping the temperature and pressure fixed at 100 K and 100 kbar, respectively. The magnetic field provides an added confinement and can be used to alter the confinement of electron–hole pairs. The applied magnetic field also lifts the energy degeneracy. The confinement frequency of the hole is kept at 3.95×10^{13} Hz. The dashed black line is the normal absorption and dispersion curve in the QD system when the coupler field is not switched on for $B = 0$ T. A TW opens up when the coupler field is ignited. Further, from figure 3, the change in crest values of susceptibilities can also be examined with a change in values of field strength. There are two ways to explain this observation. First, as B increases, the confinement of charge carriers decreases, due to which there is a decrease in the effective quantum length of the QD and hence wave functions squeeze in a smaller region. Secondly, while the coupler laser field is held at a constant value equal to 1.54×10^9 V/m, the coupler field Rabi frequency decreases with augmentation in external field strength. Both expositions result in decreased overlap of different exciton states, and subsequently $\mu_{e1,g}$ falls. As the change in crest values of real and imaginary parts of χ largely comes from the changes in the square of the dipole transition matrix element, the magnitude of crest values decreases with B. Further, it is observed that on increasing the strength of the field, separation between energy levels gets enhanced inside the QD, causing an increase in excitonic transition energies. This results in a blue-shift of susceptibility curves with enhancement in magnetic field strength. However, the width of the TW is not much affected by B.

In figure 4, we present the variation of real and imaginary parts of susceptibility of an excitonic QD for different sizes of QD. As the size of QD increases, there is an increase in the crest values of real and

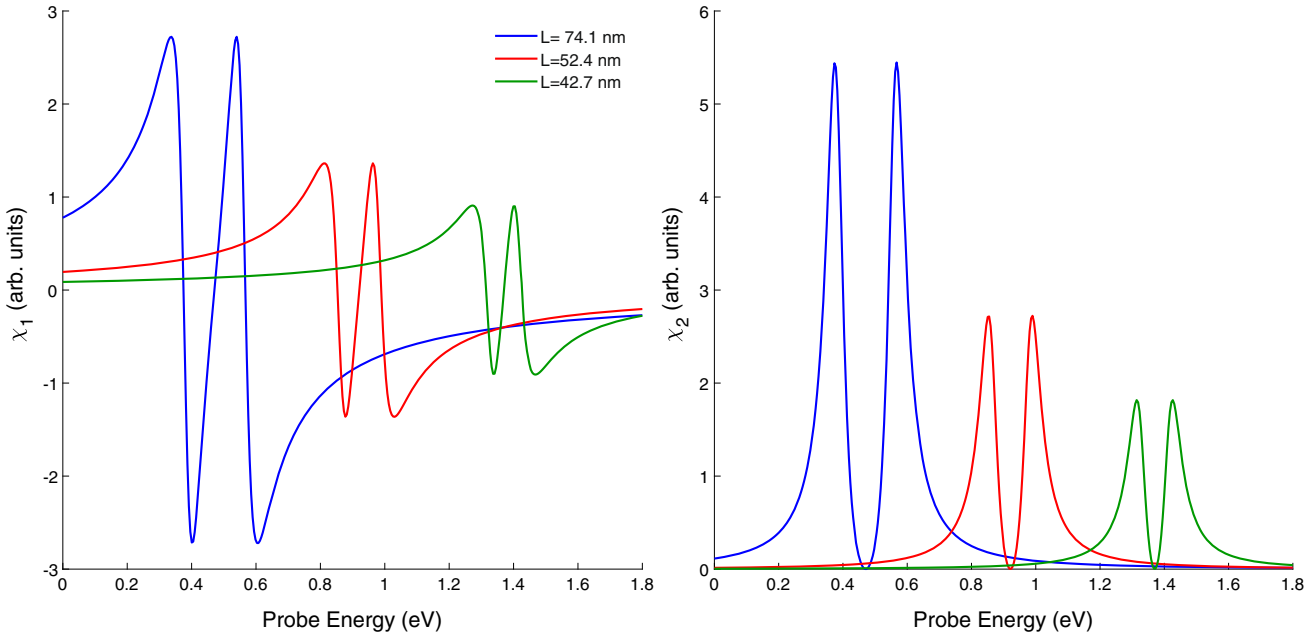

Figure 4. Variation of χ_1 and χ_2 with the energy of the probe field for different sizes of QD.

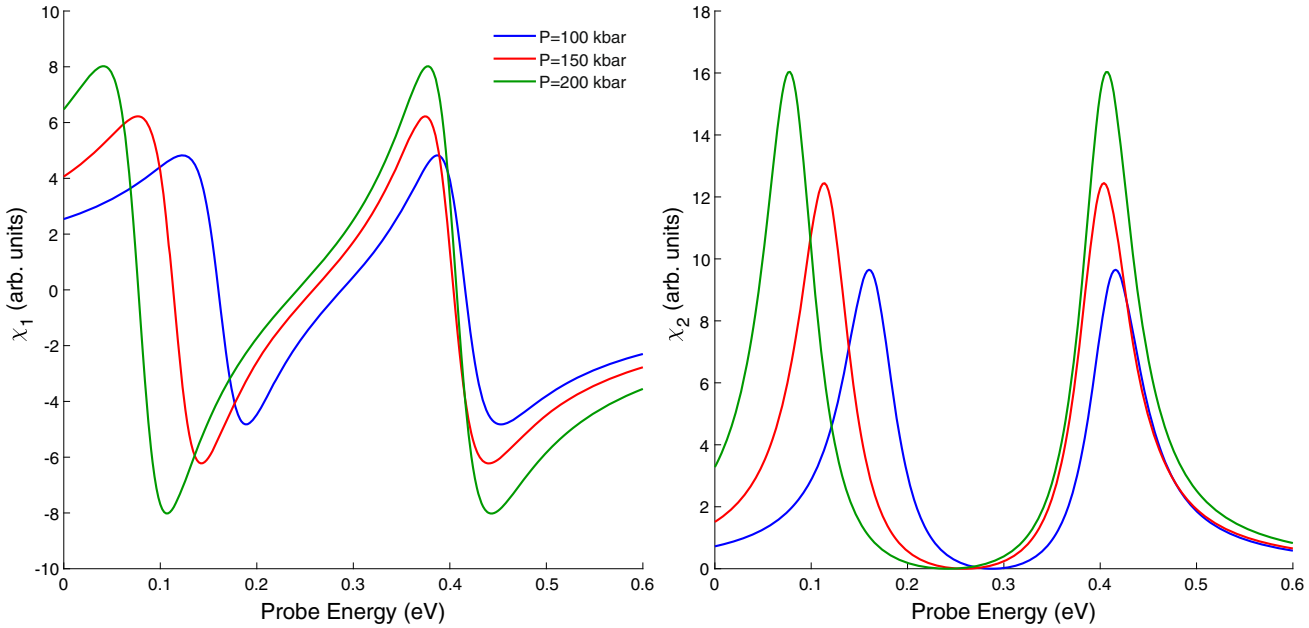

Figure 5. The variation of χ_1 and χ_2 with the energy of the probe field for different values of hydrostatic pressure.

imaginary parts of susceptibility. Further, EIT occurs at lower probe energies. The physical reason behind this is that as the dimension of QD increases, the transition energies decrease as the excitons are now bound in small space and hence curves shift to lower probe energies (red-shift). Additionally, the increase in quantum confinement leads to an increase in dipole matrix elements, due to which crest values increase. The TW gets finer as the size of QD reduces. Similar results are obtained by Azizi and Vaseghi [39] in the QD system.

In figure 5, we plot the variation of susceptibilities of an excitonic QD as a function of $\hbar\omega_p$ for different values of hydrostatic pressure keeping the temperature constant at 200 K. The figures show that an increase in pressure increases the crest values of χ_1 and χ_2 and moves them toward lower probe energy values. By analysing eqs (22)

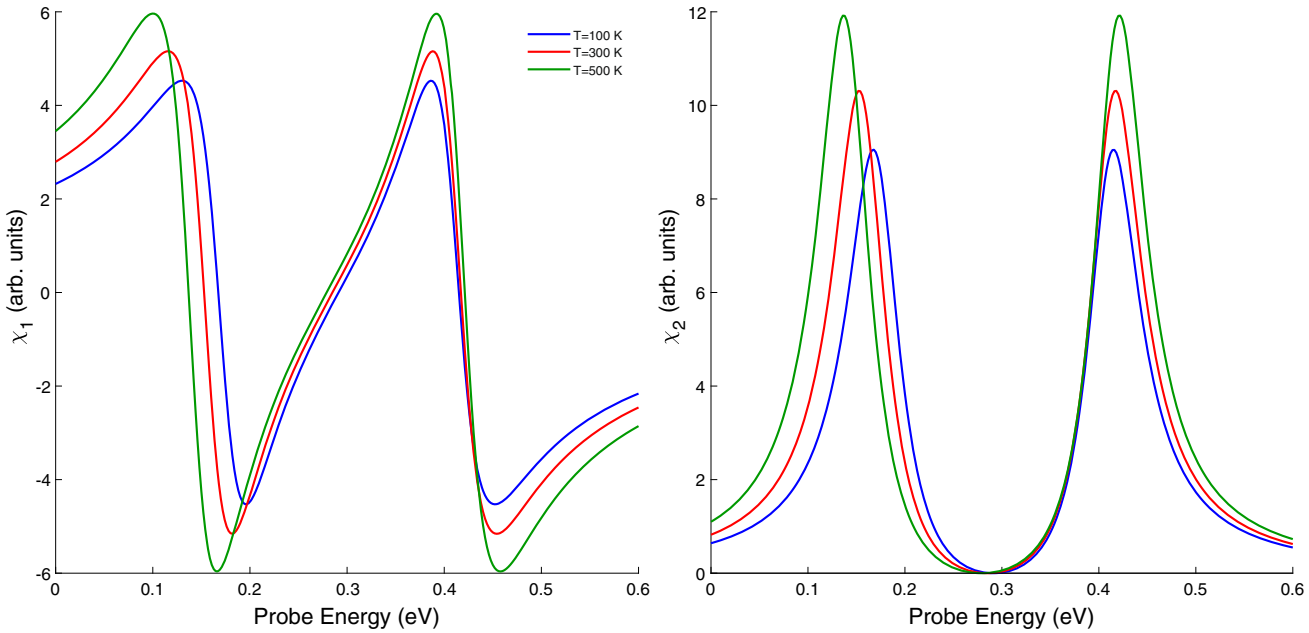

Figure 6. Variation of χ_1 and χ_2 with the energy of the probe field for different values of temperature.

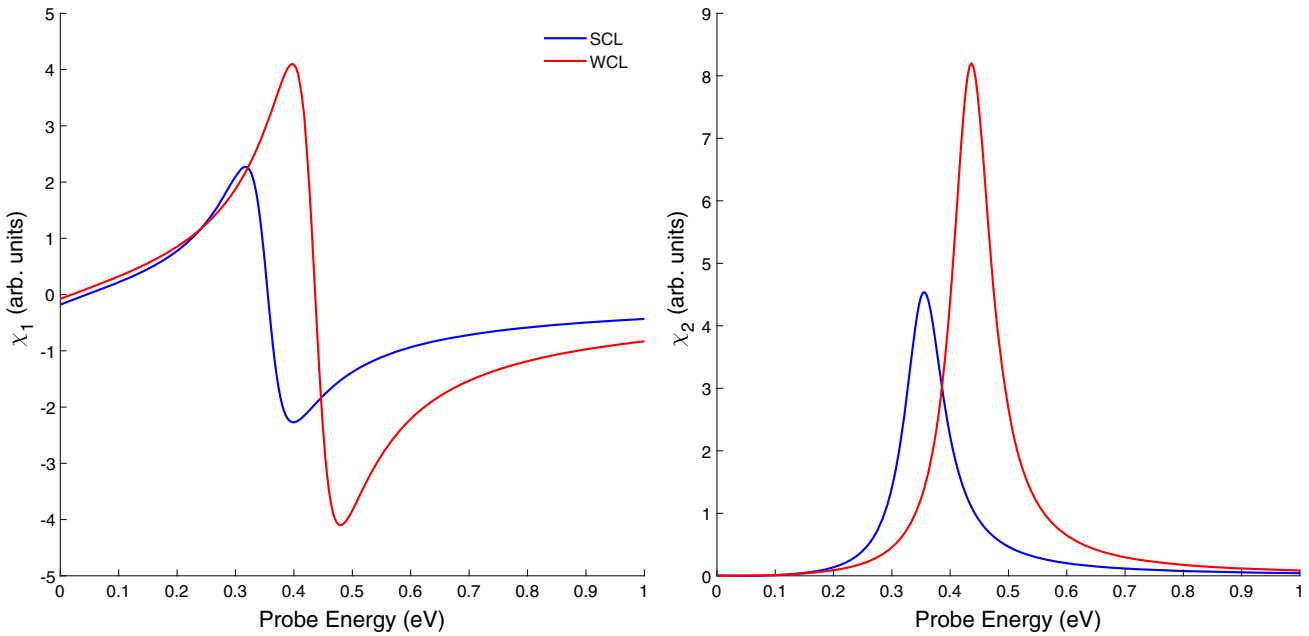

Figure 7. Variation of χ_1 and χ_2 with the energy of the probe field for SCL and WCL.

and (23), it can be seen that the red- or blue-shift of the curves is mainly associated with the energy separation of levels associated with the transition. $\Delta E_{e1,g}$, in principle, should increase and $|\mu_{e1,g}|$ should decrease with increasing pressure owing to an increase in confinement. However, in our study, we found that as the pressure increases, the reverse happens that induces a red-shift in the curves and an increase in crest values. This may be attributed to the fact that both the dielectric constant and effective masses of the confined electron and hole also have functional dependence on pressure and temperature, in addition to quantum confinement. In our problem, it is observed that the effect of effective masses of electron and hole dominates over quantum confinement effect. An increase (decrease) in pressure increases the effective masses of the electron (hole) so that the reduced mass of electron and hole, μ, decreases. This increases the effective QD length as L depends on μ, the reduced mass of electron and hole. This decreases the confinement effect, inducing a

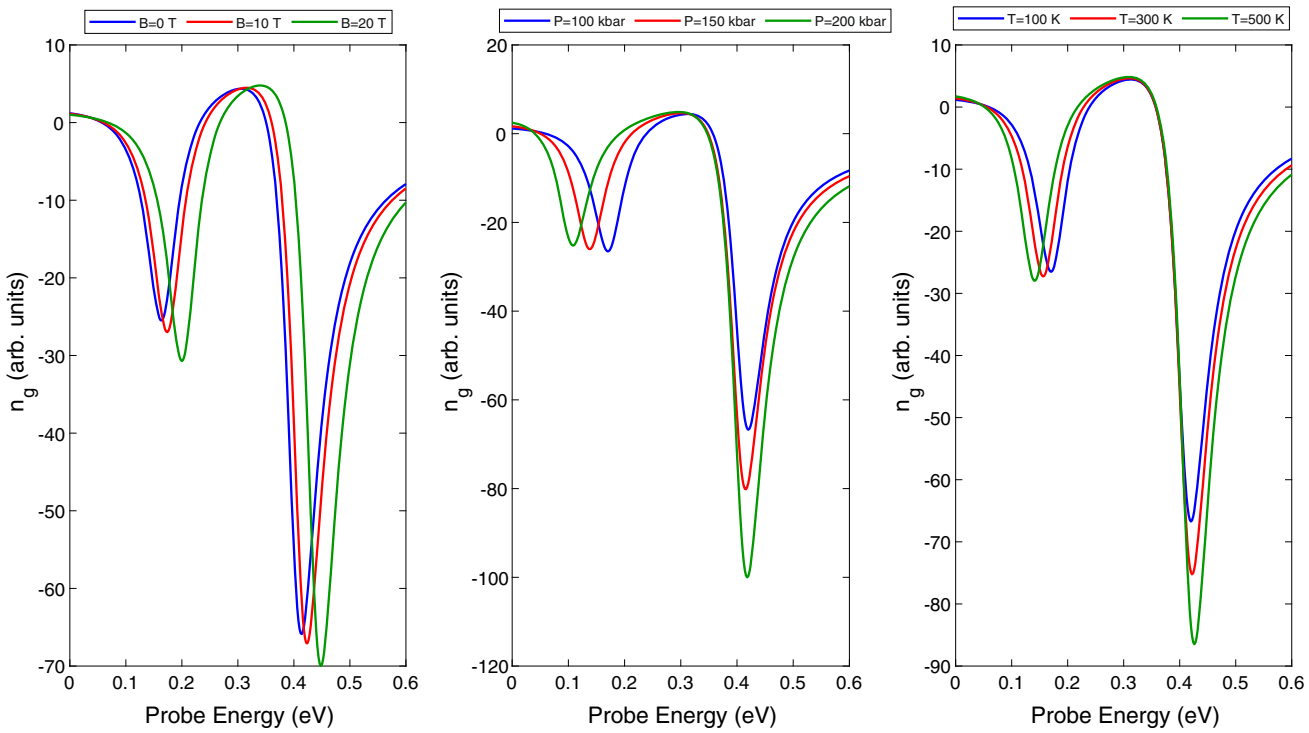

Figure 8. Plots of the GI with the probe field energy for the magnetic field, hydrostatic pressure and temperature changes.

red-shift in their crest positions and a fall in their crest values, as can be observed in figure 5. Thus, effective masses of charge carriers and dielectric constant play a major role in manipulating the effective size of QD. The TW also expands with increasing pressure.

In figure 6, we plot the variation of absorption and dispersion spectra of the system with probe energy for different values of temperature. The figure shows that as temperature increases, the crest values of absorption and dispersion curves increase and positions suffer red-shift. This occurs because as temperature increases, the reduced mass falls off. As already discussed, this results in the increase of the effective length of QD that shifts the crest positions towards low energies and increase in their magnitudes.

In figure 7 we plot the variation for χ_1 and χ_2 with probe field energy in two different limits: SCL and WCL. In SCL, the impact of the carrier confinement is more significant than the effects related to the electrostatic interaction. Due to the strong confinement of carriers, the electrostatic interaction between electrons and holes can be ignored, thereby carriers are bound in a smaller QD and excitonic energy level spacing is large. In the WCL, the excitonic level spacing decreases due to which the curve suffers blue-shift. Further, in SCL, due to an increase in carrier confinement, the wave function is now spread in a smaller QD, which results in the decreasing behaviour of the dipole matrix elements and height of the susceptibility crests.

Figure 8 shows the variation of GI, n_g, with the variation in magnetic field, pressure and temperature. In every case, if $n_g > 1$, the group velocity of the incident radiation is small compared to c, thus the propagation of radiation is subluminal. However, if $0 < n_g < 1$, the group velocity of the radiation is larger than c or it becomes negative, thus the propagation of radiation is superluminal. In every variation shown above, the group velocity of a light pulse can be determined by the slope of χ_2 or the dispersion curve. The negative slope of dispersion corresponds to superluminal light propagation, while the positive slope shows subluminal light propagation. The application of the magnetic field does not have a noticeable impact on TW and the width of TW is almost unchanged. Thus, the sub and superluminal frequency intervals remain stable but show a blue shift with increasing magnetic field. For other results, the variation in GI can be explained by variation in the slope of χ_2. Subluminal and superluminal frequency intervals are also affected by the changes in pressure and temperature and they display the same effects as exhibited in figures 5 and 6. The physical reasons behind these results have already been explained.

4. Conclusion

In summary, we calculated the energy eigenvalues, the corresponding wave functions and dipole matrix

elements of an exciton confined in a spherical QD in the presence of static magnetic field. The results obtained are exploited to understand the process of EIT and explore the effects of external factors, specifically external static magnetic field, hydrostatic pressure and temperature on the EIT and the GI of a probe laser light. The effect of QD dimensions and confinement limits of exciton are also examined. The results are peculiar to the process of EIT. The forte of our paper is the simplicity of calculations taking into account electrostatic Coulomb interaction between electron and hole. We anticipate that it will strengthen our understanding of the optical properties of confined excitons in quantum nanostructures and beneficial towards manufacturing various optoelectronic devices.

References

[1] S Mo, K Guo, G Liu, X He, J Lan and Z Zhou, *Thin Solid Films* **710**, 138286 (2020)
[2] Varsha, M Kria, J El Hamdaoui, L M Pérez, V Prasad, M El-Yadri, D Laroze and E M Feddi, *Nanomaterials* **11**, 1513 (2021)
[3] M K Elsaid, A A Alia and A Shaer, *Chin. J. Phys*. **66**, 335 (2020)
[4] B-J Liu and M-H Yung, *Quantum Sci. Technol*. **6**, (2021)
[5] T Okamoto, N Fujimura, L Crespi, T Kodera and Y Kawano, *Sci. Rep*. **9**, 18574 (2019)
[6] P Hosseinpour, *Phys. B Condens. Matter* **613**, 412973 (2021)
[7] R G Beausoleil, W J Munro, D A Rodrigues and T P Spiller, *J. Mod. Opt*. **51**, 2441 (2004)
[8] H-C Li, G-Q Ge and M S Zubairy, *Phys. Rev. A* **102**, 053701 (2020)
[9] Zhao Chen, Xiaokang Song, Rongzhen Jiao, Gaoyan Duan, Lulu Wang and Li Yu, *IEEE Photon. J.* **7**, 1 (2015)
[10] Z Wei, X Li, N Zhong, X Tan, X Zhang, H Liu, H Meng and R Liang, *Plasmonics* **12**, 641 (2017)
[11] X-J He, L Wang, J-M Wang, X-H Tian, J-X Jiang and Z-X Geng, *J. Phys. D: Appl. Phys.* **46**, 365302 (2013)
[12] Q Wang, L Yu, H Gao, S Chu and W Peng, *Opt. Express* **27**, 35012 (2019)
[13] J Shiri, *Laser Phys*. **29**, 056202 (2019)
[14] A Imamoğlu and S E Harris, *Opt. Lett.* **14**, 1344 (1989)
[15] S E Harris, J E Field and A Imamoğlu, *Phys. Rev. Lett.* **64**, 1107 (1990)
[16] M C Phillips and H Wang, *Phys. Rev. B* **69**, 115337 (2004)
[17] E Sahebi, H R Askari and B Behroozian, *Optik* **185**, 339 **(2019)**
[18] M Gambhir, S Gumber, P K Jha and M Mohan, *Superlatt. Microstruct*. **71**, 147 (2014)
[19] E C Niculescu, *Chem. Phys*. **487**, 16 (2017)
[20] D Bejan, *Eur. Phys. J. B* **90**, 54 (2017)
[21] D Bejan, *Opt. Mater.* **67**, 145 (2017)
[22] A Ouadgui, J Diouri and J Khamkhami, *Pramana – J. Phys.* **94**, 30 (2020)
[23] M Gambhir and V Prasad, *Chin. Phys. B* **28**, 087803 (2019)
[24] S Nasa and S P Purohit, *Phys. E: Low-Dimens. Syst. Nanostructures* **118**, 113913 (2020)
[25] J-F You, Q Zhao, Z-H Zhang, J-H Yuan, K-X Guo and E Feddi, *Int. J. Mod. Phys. B* **33**, 1950325 (2019)
[26] B Akbarnavaz Farkoush, G Safarpour and A Zamani, *Superlatt. Microstruct*. **59**, 66 (2013)
[27] N Aghoutane, L M Pérez, A Tiutiunnyk, D Laroze, S Baskoutas, F Dujardin, A El Fatimy, M El-Yadri and E M Feddi, *Appl. Sci.* **11**, 5969 (2021)
[28] W Wang, L Xu, X Wei, S Zhang and Z Yao, *J. Appl. Phys*. **127**, 195903 (2020)
[29] A John Peter, *Phys. E: Low-Dimens. Syst. Nanostructures* **28**, 225 (2005)
[30] M Gambhir and V Prasad, *J. Mod. Opt*. **68**, 542 (2021)
[31] S Wielandy and A L Gaeta, *Phys. Rev. A* **58**, 2500 (1998)
[32] B Nguyen Huy, D Le Van and K Dinh Xuan, *Commun. Phys*. **29**, 1 (2019)
[33] J Gea-Banacloche, Y Li, S Jin and M Xiao, *Phys. Rev. A* **51**, 576 (1995)
[34] S E Harris and L V Hau, *Phys. Rev. Lett*. **82**, 4611 (1999)
[35] L V Hau, S E Harris, Z Dutton and C H Behroozi, *Nature* **397**, 594 (1999)
[36] A V Turukhin, V S Sudarshanam, M S Shahriar, J A Musser, B S Ham and P R Hemmer, *Phys. Rev. Lett*. **88**, 023602 (2001)
[37] C M Duque, M E Mora-Ramos and C A Duque, *J. Nanopart. Res*. **13**, 6103 (2011)
[38] A El Moussaouy, N Ouchani, Y El Hassouani and D Abouelaoualim, *Superlatt. Microstruct*. **73**, 22 (2014)
[39] V Azizi and B Vaseghi, *Opt. Quant. Electron*. **50**, 93 (2018)